Visual Abstract

# Influence of 3D-printing parameters on the mechanical properties of 17-4PH stainless steel produced through Selective Laser Melting

Francesca Romana Andreacola, Ilaria Capasso, Letizia Pilotti, Giuseppe Brando

*Department of Engineering and Geology, University "G. d'Annunzio" of Chieti-Pescara, Viale Pindaro, 42, 65127 Pescara, Italy*
*francesca.andreacola@unich.it*
*ilaria.capasso@unich.it, https://orcid.org/0000-0002-7536-404X*
*letizia.pilotti@unich.it*
*giuseppe.brando@unich.it, https://orcid.org/0000-0003-3169-516X*

OPEN ACCESS

**ABSTRACT.** Additive Manufacturing (AM) is a technological process in which elements are fruitfully built-up adding materials layer by layer.

AM had a massive development in recent times, thanks to its intrinsic advantages, especially if compared with conventional processes (i.e. subtractive manufacturing methods), in terms of free-form design, high customization of products, a significant reduction in raw materials consumption, low request of postprocessing and heat treatments, use of pure materials and reduced time for final products to be marketed.

In order to give an innovative contribution to the knowledge in the field of metal AM materials, this paper reports the main outcomes of an experimental campaign focused on the influence of several specific printing parameters on the mechanical features of the 17-4PH stainless steel, which is one of the most used metal for the Selective Laser Melting (SLM) technology. The influence of different printing directions and sample inclinations on the material mechanical behavior is assessed, with the aim of considering an innovative use in the field of structural engineering. Moreover, the effects due to scanning and recoating times are studied. In addition, the consequences of heat treatment (annealing) on both the residual stresses and the amount of residual austenite are appraised.

**KEYWORDS.** Selective Laser Melting (SLM); 17-4PH stainless steel; Tensile test; 3D-printing parameters; Mechanical properties; Additive Manufacturing.

## INTRODUCTION

Additive Manufacturing (AM), also known as 3-D Printing, is a technology based on the addition of material, superimposed layer by layer, to create pieces or parts of them. This method positively exploits the possibility of direct interfacing with CAD (Computer Aided Design), CAM (Computer Aided Manufacturing) and CNC (Computer Numerical Control) software [1], for easily obtaining free-form elements.

During the last 30 years, AM has had a groundbreaking development thanks to its irrefutable advantages, such as its versatility in reproducing whatever geometry, the minimum human interaction requirement, the reduced time of design [2], etc.

The development of the current AM process passed through different printing technologies proposed in the last decades, which are summarized in Fig. 1 [2–6]: in 1980 SLS (Selective Laser Sintering) systems were developed; in 1986, Hull patented a manufacturing process called SLA (Stereolithography); in 1988, LOM (Laminated Object Manufacturing) systems were developed; in 1989, the first FDM (Fused Deposition Modeling) machine was marketed; in 1995, the first SLM (Selective Laser Melting) machines were proposed as an alternative technology to stereolithography; in 1998, Arcam AB marketed the first EBM (Electron Laser Melting) based machine. Since early 2000, several different 3D Printing machines and techniques were developed, and, in the last years, a relevant diffusion of new methodologies, with a significant research effort for using innovative materials, has been recorded worldwide (see Tab. 1).
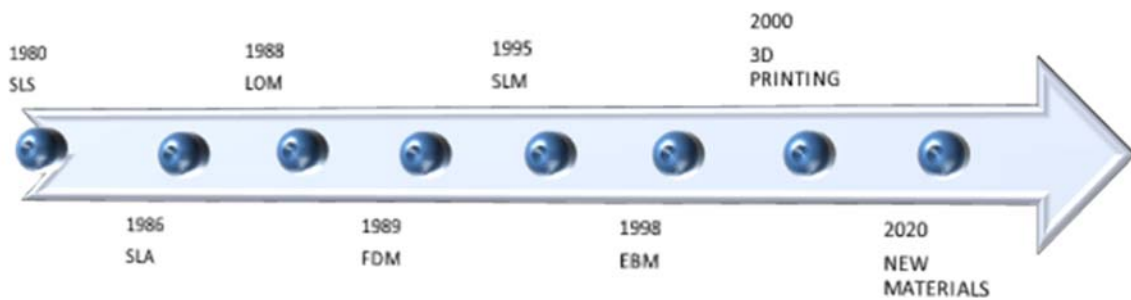


Figure 1: Evolution of the Additive Manufacturing technology.

| Solid based | Liquid based | Powder based |
|---|---|---|
| Fused Deposition Modeling (FDM) | Stereolithography (SLA) | Selective Laser Melting (SLM) |
| Laminated Object Manufacturing (LOM) | Multi-Jet Modeling (MJM) | Electron Beam Melting (EBM) |
| | Digital Light Processing (DLP) | Selective Laser Sintering (SLS) |
| | Multi-Jet Modeling (MJM) | Laser Metal Deposition (LMD) |
| | | Laser Engineered Net Shaping (LENS) |

Table 1: Classification of AM process depending on the state of raw material [3][7].

Nowadays, the different types of AM (Additive Manufacturing) processes should be rely on the material used, on the methods adopted for building the layers and on the applications required from the beginning to the end of the process. A CAD (Computer aided design) representation of the object is the starting point for any AM process. The quality of the model directly affects the final result for which an accurate virtual representation phase is essential. However, nowadays, there are several methods for obtaining a CAD representation even for non-experts of virtual modeling software.

Once the CAD file is obtained, the following step is to make it readable for the printer. For this purpose, all the machines need to convert the CAD model into an STL (Standard Triangulation Language) file, a Stereolithography interface format, and then perform the object slicing [3].

Among the available AM processes, SLM has attracted attention more and more in the last recent years, because of its superior flexible manufacturing capability, with fruitful applications in the aerospace, medical, and automotive industries. This AM technology uses a high-energy laser beam, by which the piece is built layer-by-layer through the selective melting and consolidation of a metal powder. The layer thicknesses vary in the range of 20 and 100 µm. Compared with the traditional casting and forging methods, SLM attracted and attracts increasing attention due to its outstanding features, such as the ability to net-shape manufacture without the dies and the high capacity of manufacturing any geometry. The SLM process is schematically shown in Fig. 2.

The laser beam is mounted on the top of the machine and a set of deflection and focus lenses concentrates the beam itself on the material powder bed for the solidification of the layers. Once a layer is sintered a building plate goes down and the roller delivers a new layer on the top of the bed. This process continues, layer by layer until the object is complete as designed. Further details on the advantages and disadvantages of this technology are shown in Tab. 2 [3].
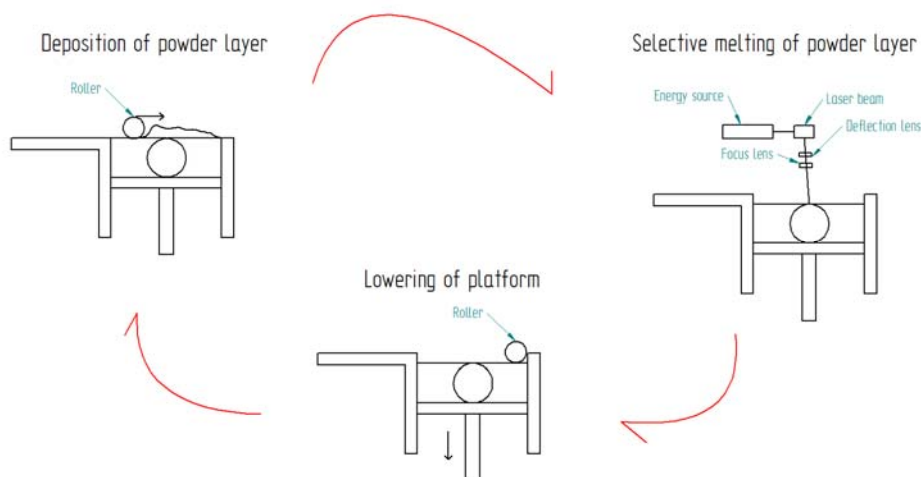


Figure 2: Schematization of the SLM process.

In the framing of wider research activity, focused on the implementation of AM processes for the manufacturing of special devices for the seismic protection of buildings, this paper presents the first outcomes of an experimental campaign conceived to identify the relation of the mechanical behavior of base material and some of the meaningful printing parameters, i.e. the recoating time, the printing direction and the orientation of the parts on the plate during the production process.

| Advantages | Disadvantages |
|---|---|
| Use of pure materials | Mainly industrial techniques |
| High density | Hight processing temperatures |
| No subsequent treatments are required | High machinery costs |
| Ability to create non-Euclidean forms | |
| Excellent mechanical performance | |

Table 2: Advantages and disadvantages of SLM [8].

The investigated material is the 17-4 Precipitation Hardening stainless steel. The scope of the testing activity is to detect the optimum printing parameters that will be used for the continuation of the research activity.
Apart from the tensile tests that will be presented in the paper, also X-ray diffraction analyses will be shown, in order to investigate the effects of residual stresses on metallography and on the microstructural and crystalline composition of the material.
The reported analyses have been carried out on coupons either with or without heat treatment, so to emphasize the influence of this process that usually is implemented to reduce the residual stresses developed during the additive manufacturing process and to increase the material ductility.

## MATERIALS AND METHODS

### Manufacturing conditions

A Selective Laser Melting system (SLM 280) from SLM Solutions GmbH (Lubeck, Germany) was used for the production of the specimens. The machine has a laser beam (Yb-Fiber Laser) with a power limit of 400 W and offers a 280 x 280 x 320 mm build envelope. The inert atmosphere inside the construction chamber is guaranteed

by the presence of Argon gas and the temperature can reach 65 °C. Instead, the temperature of the building plate throughout the entire manufacturing process can be increased up to 150 °C.

For the experimental tests described in this paper, the following processing parameters were applied:

– Laser beam diameter: 75 µm
– Laser beam power: 200 W
– Laser scanning speed: 800 mm/s
– Layer thickness: 30 µm
– Laser scanline spacing: 80 µm
– Hatch distance: 120 µm
– Minimum scanning time variable
– Stripes scanning strategy

The selected platform temperature during the printing process was 100 °C while the temperature inside the construction chamber varied between room temperature in the initial phase and 30-35 °C during the additive manufacturing process. When the printing process was completed, the specimens were not subjected to any surface treatment, but only polished after removing the supports. Fig. 3 shows a detail of the samples as soon as the additive manufacturing process is complete.
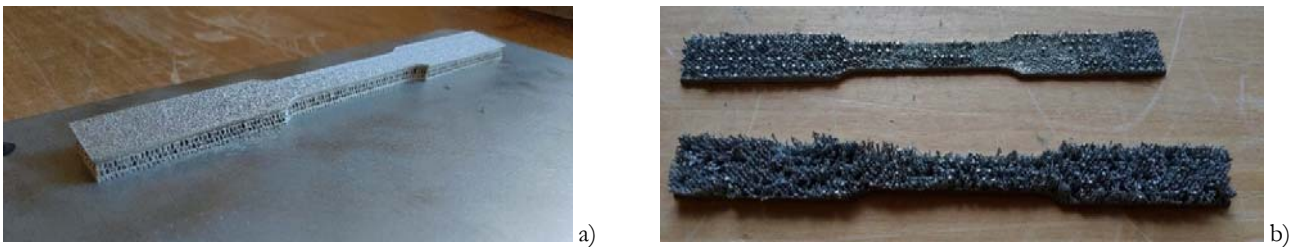


Figure 3: Specimens after printing process: a) Specimen on the building plate with its supports; b) Detail of the support structures located at the bottom of the specimen, required for printability in the additive manufacturing process.

*The studied specimens*

The material used for this study is 17-4PH stainless steel, also known as 630 steel according to the AISI standard, which is one of the most used steel alloys in additive manufacturing [9–11]. It is a precipitation-hardened stainless steel with high yield strength, good corrosion resistance and high wear resistance [12–15].

An overview of the physical properties of the raw 17-4PH stainless steel powder, provided by SLM Solutions, is reported in Tab. 3, whereas in Tab. 4 the nominal mechanical features of the printed metal for two different printing directions are listed [16]. Furthermore, Tab. 5 shows the chemical composition of the feedstock [16].

| Property | Value |
|---|---|
| Mass density | 7.8 g/cm³ |
| Thermal conductivity (at 20° C) | 16 W/(m·K) |
| Component density | > 99.5 % |
| Built-up rate (theoretical value) | 16.85 cm³/h |
| Particle size | 10 – 45 µm |
| Particle shape | Spherical |

Table 3: Nominal physical properties of 17-4PH powder material.

| Mechanical Properties | Printing Direction | As-built | Heat-treated |
|---|---|---|---|
| Young's Modulus E | 0° | 171 MPa | 154 MPa |
| | 90° | 154 MPa | 182 MPa |
| Yield strength $\sigma_y$ | 0° | 517 MPa | 1024 MPa |
| | 90° | 506 MPa | 1391 MPa |
| Ultimate tensile strength $\sigma_u$ | 0° | 987 MPa | 1359 MPa |
| | 90° | 931 MPa | 1308 MPa |
| Elongation at break $\varepsilon_u$ | 0° | 26 % | 16 % |
| | 90° | 28 % | 14 % |
| Reduction of area $\Delta_A$ | 0° | 56 % | 27 % |
| | 90° | 56 % | 26 % |

Table 4: Nominal mechanical properties of 17-4PH stainless steel.

| Fe | Cr | Ni | Cu | Mn | Si | Nb + Ta | C | N | O | P | S |
|---|---|---|---|---|---|---|---|---|---|---|---|
| Balance | 15.0/17.5 | 3-5 | 3-5 | 1 | 0.07 | 0.15/0.45 | 0.07 | 0.1 | 0.04 | 0.04 | 0.015 |

Table 5: Chemical composition of 17-4PH powder.

Two groups of specimens, for a total of 30 samples, were manufactured to be subjected to tensile tests, in order to assess how the production process and its parameters affect the mechanical properties [15].

The first group, which was not produced according to a Standard, was used as a preliminary investigation to test the printer machine and to evaluate the surface finish of the additive manufactured material and the differences in terms of the final result of samples produced with different orientations and/or inclinations. The dimensions and the geometrical features of these not-standardized samples are shown in Fig. 4.
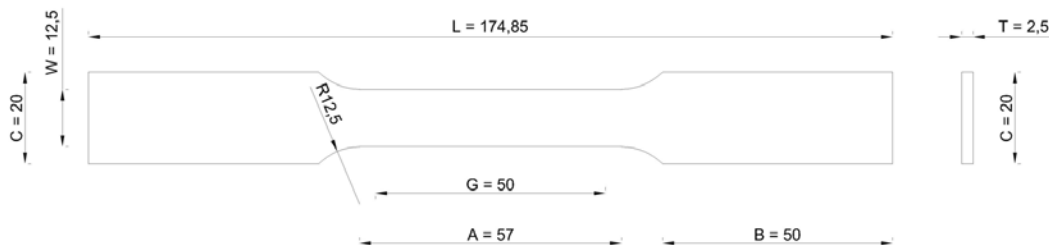


Figure 4: Geometric dimensions of the first group of tensile test specimens.

The specimens were printed in three different directions. Two directions with the longitudinal axis parallel to the x-y plane (horizontal, 5° and 85° inclined) and one with the longitudinal axis perpendicular to the x-y plane (vertical) were considered. It should be noted, however, that all the samples were printed with an inclination of 5° concerning the considered direction, in order to limit the negative effects of the additive manufacturing process on the angles using this slight inclination to reduce area overhangs.

A summary of the first group of samples, with positioning details for all different configurations, is reported in Tab. 6, where details about the processing direction, the specimen location on the building plate, the possible application of heat treatment processes (an annealing treatment keeping samples in an oven at a temperature of 650 °C for 2 hours and then cooling until room temperature is reached inside the switched-off oven [12,13,15]) are given.

The second group of samples was designed according to the specifications given by ASTM A370 – "Standard Test Methods and Definitions for Mechanical Testing of Steel Products" [18]. The dimensions and the geometrical features of the standardized samples are shown in Fig. 5.

Tab. 7 shows the characteristics of the second group of samples. In this case, also the scanning time, namely the time required for the fusion (i.e. the realization of one of the powder layers), was considered as a printing parameter to be

controlled: three different scanning speeds, respectively 45, 50 and 65 seconds, were performed on specimens horizontal inclined by 5° [17,19].

Moreover, in Tab. 7 the applied recoating time, i.e. time that the laser beam takes to return to its initial position once the production of a layer is complete, is specified [17].

| Specimen ID | Building direction | Amount of samples | Heat treatment | Scanning time | Recoating time |
|---|---|---|---|---|---|
| G1_17-4_TO5_N(1,2,3) | Horizontal, 5° inclined | 3 | No | N.A. | N.A. |
| G1_17-4_TO85_N(1,2,3) | Horizontal, 85° inclined | 3 | No | N.A. | N.A. |
| G1_17-4_TV_N(1,2,3) | Vertical | 3 | No | N.A. | N.A. |
| G1_17-4_TO5_HT_N4 | Horizontal, 5° inclined | 1 | Yes | N.A. | N.A. |
| G1_17-4_TO85_HT_N4 | Horizontal, 85° inclined | 1 | Yes | N.A. | N.A. |
| G1_17-4_TV_HT_N4 | Vertical | 1 | Yes | N.A. | N.A. |

\* N.A. = Not Available.

Table 6: Summary of the first group of tensile test specimens characteristics.
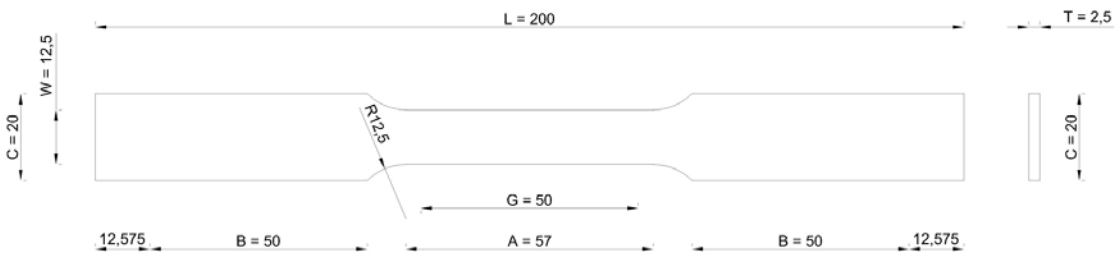


Figure 5: Geometric dimensions of the second group of tensile test specimens.

| Specimen ID | Building direction | Amount of samples | Heat treatment | Scanning time | Recoating time |
|---|---|---|---|---|---|
| G2_17-4_TO5_45_N(1,2,3) | Horizontal, 5° inclined | 3 | No | 45 | 8 |
| G2_17-4_TO5_50_N(1,2,3) | Horizontal, 5° inclined | 3 | No | 50 | 8 |
| G2_17-4_TO5_65_N(1,2,3) | Horizontal, 5° inclined | 3 | No | 65 | 8 |
| G2_17-4_TO5_45_HT_N(4,5,6) | Horizontal, 5° inclined | 3 | Yes | 45 | 8 |
| G2_17-4_TO5_50_HT_N(4,5,6) | Horizontal, 5° inclined | 3 | Yes | 50 | 8 |
| G2_17-4_TO5_65_HT_N(4,5,6) | Horizontal, 5° inclined | 3 | Yes | 65 | 8 |

Table 7: Summary of the second group of tensile test specimens characteristics.

All specimens present the typical "dog-bone" shape with a 2.5 mm thick rectangular cross-section. Fig. 6 shows some of the samples produced for both groups.
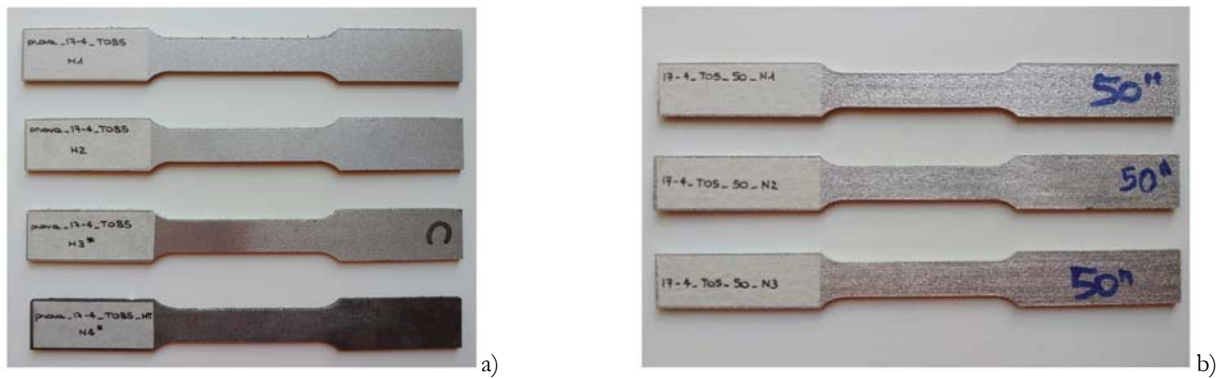
Figure 6: Some of the produced SLM 17-4PH stainless steel specimens: a) First and b) Second group of coupons.

*Mechanical characterization*

Tensile tests were performed at room temperature using a Galdabini Sun60 universal testing machine (see Fig. 7) with a maximum load capacity of 600 kN. Tests were executed in speed control, setting a speed of 6 mm/min. There is no set applied load limit, so the test ends with the specimen breaking. A summary of the experimental tests setup is provided in Tab. 8.

Moreover, Penny & Giles linear displacement sensors were employed to measure the deformation of the specimens. These devices, connected to an electronic control unit, are able to monitor stroke lengths ranging of up to 100 mm.



Figure 7: Tensile testing machine detail.

*Evaluation of residual stresses*

In order to evaluate the residual stresses, X-ray diffraction (XRD) analyses were carried out for both heat-treated and not heat-treated samples. A GNR StressX system was used for this purpose.

Residual stresses arising during 3d printing are mainly due to the high cooling rate of the layers and could affect the mechanical performance of final products [20,21].

The determination of the residual stresses was performed by X-ray diffraction with a Cr kα radiation, within the ψ range from -40° to +40° with a step size of 30-60 s.

Also, the amount of residual austenite was evaluated by means of XRD analysis through the GNR ArexD solution. It is known that its presence, even in small percentages (5%), can cause unexpected deformations that modify the mechanical properties of printed parts [9,12,13]. The percentage amount of austenite was also considered on the virgin powder raw material. The phases of samples were conducted by X-ray diffraction with a Point focus Molybdenum anode, within the 2θ range from 21.5° to 44.5° with an acquisition time of 180 s.

| Test parameters | Settings |
|---|---|
| Control type | Speed control |
| Load application speed | 6 mm/min |
| Maximum load | 600 kN |
| Load limit | No |
| Preload | No |
| Gauge length $L_0$ | 50 mm |
| Crosshead speed | 300 mm/min |
| Unloading speed | 3 mm/min |
| End-of-test mode | Sample failure |
| Test temperature | Room temperature |

Table 8: Test machine specifications and test conditions.

## RESULTS AND DISCUSSION

*Tensile tests results*

Stress-strain curves of the vertically and 5° and 85° horizontally oriented coupons are shown in Fig. 9, whereas the stress–strain curves of the samples produced with scanning times (T) of 45 s, 50 s, and 65 s are shown in Fig. 10. In both figures, the specimens in either their as-built or heat-treated (HT) conditions have been reported.

The values of the yield stress $\sigma_y$, the failure stress $\sigma_u$ and the failure strain $\varepsilon_u$ for both sets of samples are summarized in Tabs. 9 and 10. Both tables contain the average results of the mechanical parameters obtained for each type of specimens and their standard deviation values (SD). Fig. 8 displays a detail of the samples during the tests execution.



Figure 8: Detail of tensile test execution: a) Specimen before the start of the test; b) Specimen at the end of the test.

*Influence of printing direction*

The yield strength presents average values of 636 MPa, 818 MPa and 616 MPa respectively for specimens manufactured vertically, inclined by 5° and inclined by 85°.

The ultimate tensile strength does not vary significantly with the printing direction. In fact, the obtained mean values are 1282 MPa, 1314 MPa and 1296 MPa respectively for the vertically, horizontally inclined 5° and 85° samples.

The failure strain also shows no significant changes in relation to the different printing orientations. The average values recorded were 14.1% for specimens manufactured vertically and horizontally inclined by 5°, and 14.2% for specimens manufactured horizontally inclined by 85°.

*Influence of scanning time*

The yielding strain displays mean values of 751 MPa, 634 MPa and 593 MPa for samples produced respectively with scanning times of 45 s, 50 s and 65 s.
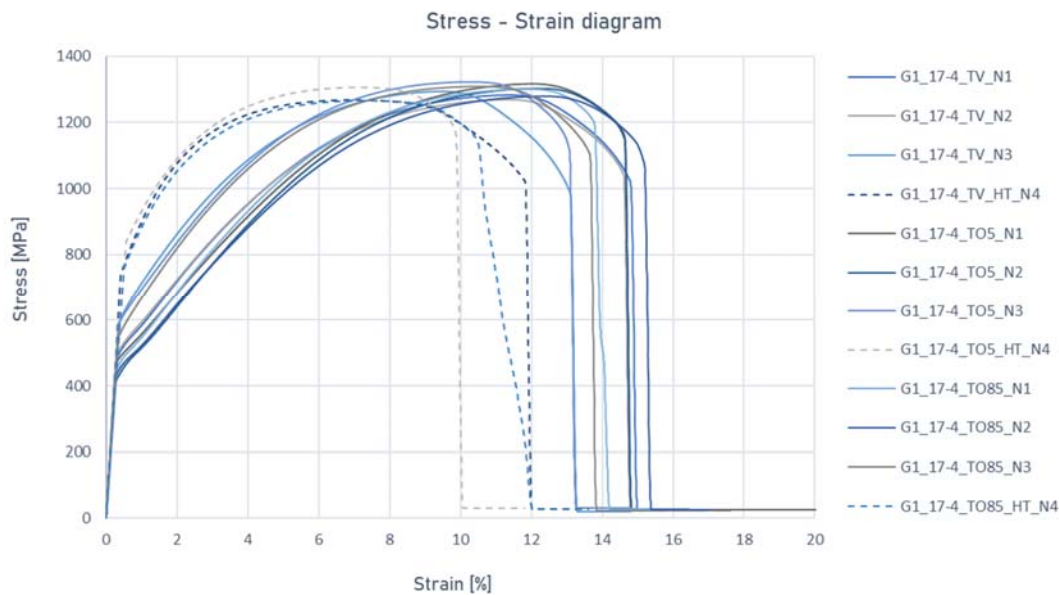


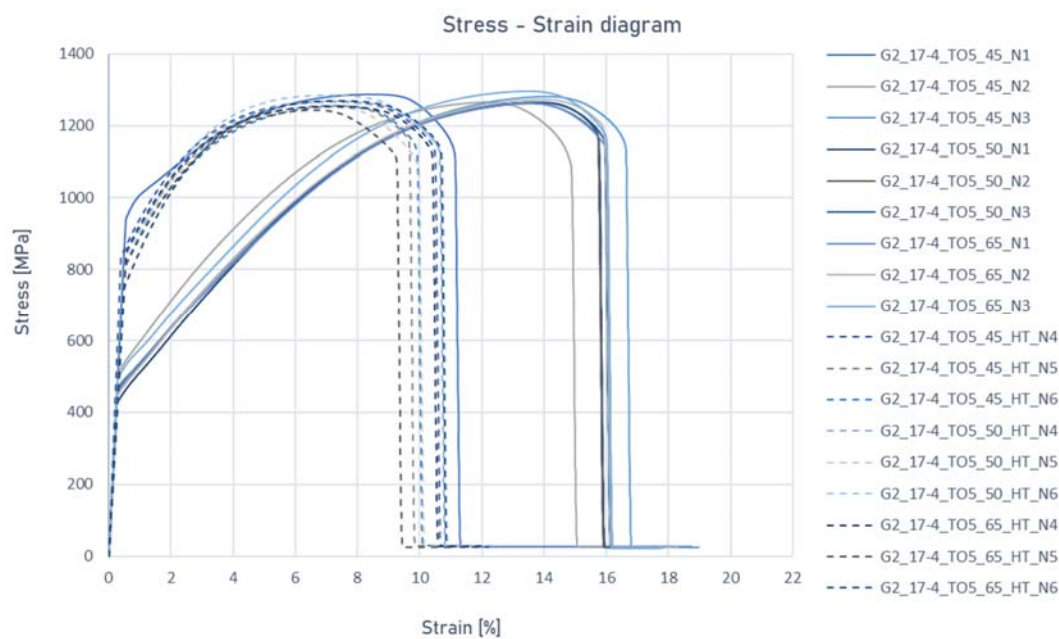Figure 9: Engineering stress–strain curves of the first group of SLM 17-4PH ss coupons produced.



Figure 10: Engineering stress–strain curves of the second group of SLM 17-4PH ss samples produced.

| Specimen ID | $\sigma_y$ MPa | SD MPa | $\sigma_u$ MPa | SD MPa | $\varepsilon_u$ % | SD % |
|---|---|---|---|---|---|---|
| G1_17-4_TO5 | 818 | ±118 | 1314 | ±8 | 14.1 | ±0.68 |
| G1_17-4_TO5_HT_N4 | 1163 | / | 1306 | / | 9.8 | / |
| G1_17-4_TO85 | 616 | ±131 | 1296 | ±13 | 14.2 | ±0.71 |
| G1_17-4_TO85_HT_N4 | 1024 | / | 1266 | / | 10.6 | / |
| G1_17-4_TV | 636 | ±81 | 1282 | ±10 | 14.1 | ±0.78 |
| G1_17-4_TV_HT_N4 | 1037 | / | 1268 | / | 11.8 | / |

Note: The average values are calculated among the as-built specimens.

Table 9: Tensile test results for the first group of specimens.

| Specimen ID | $\sigma_y$ MPa | SD MPa | $\sigma_u$ MPa | SD MPa | $\varepsilon_u$ % | SD % |
|---|---|---|---|---|---|---|
| G2_17-4_TO5_45 | 751 | ±199 | 1278 | ±9 | 14.2 | ±2.24 |
| G2_17-4_TO5_45_HT | 1116 | ±32 | 1248 | ±10 | 10.9 | ±1.51 |
| G2_17-4_TO5_50 | 634 | ±58 | 1264 | ±1 | 15.8 | ±0.12 |
| G2_17-4_TO5_50_HT | 1094 | ±32 | 1268 | ±13 | 10.4 | ±0.36 |
| G2_17-4_TO5_65 | 593 | ±51 | 1277 | ±14 | 16.0 | ±0.05 |
| G2_17-4_TO5_65_HT | 1095 | ±11 | 1255 | ±11 | 10.0 | ±0.68 |

Note: The average values are calculated both among the as-built and heat-treated specimens.

Table 10: Tensile test results for the second group of specimens.

As with the printing direction, the different scanning time does not considerably influence the results obtained in terms of failure stress. In fact, the values achieved for specimens manufactured with scanning times of 45 s, 50 s and 65 s are respectively 1278 MPa, 1264 MPa and 1277 MPa. The same consideration can be made for the failure strain which displays values of 14.2%, 15.8% and 16.0% respectively for the samples produced with scanning rates of 45 s, 50 s and 65 s.

*Effects of heat treatment on mechanical properties*

The comparison between the as-built and heat-treated specimens showed that the heat treatment changed the stress-strain behavior of the material for all types of samples with different printing features.

As far as the yield stress is concerned, it varies with different manufacturing orientations of about +63% for vertically printed specimens, of about +42% for horizontally 5° inclined specimens and of about +66% for horizontally 85° inclined specimens.

The annealing treatment induces an increase in yield strength also for samples produced with different scanning times. In particular, this parameter rises of +49%, +73% and +85% for specimens manufactured with scanning rates of 45 s, 50 s and 65 s, respectively.

With regard to failure stress, the experimental results do not change significantly due to heat treatment, both for different printing directions and different scanning speeds. In fact, failure stresses decrease of about -1.1% for vertically manufactured specimens, of about -0.6% for specimens horizontally inclined by 5° and of about -2.3% for samples horizontally inclined by 85°. Considering the different scanning rates of 45 s, 50 s and 65 s, the ultimate tensile strength changes of about -2%, +0.4% and -2%, respectively.

The heat treatment also implies a decrease in failure strain. In fact, a reduction of approximately -16.3%, -30.3% and -25.4% for the vertically, horizontally 5° and 85° inclined specimens, respectively, can be observed. Likewise, for specimens processed with scanning times of 45 s, 50 s and 65 s the failure strain varies of about -23.5%, -34.3% and -37.2%.

The values of the mechanical parameters obtained after the annealing treatment seem to be in contrast with the trend reported in the literature for steel alloys produced by conventional methods, which are generally more ductile and less resistant after heat treatments, even if beyond certain temperatures, there are no further beneficial effects. However, in addition to the data provided by the manufacturer of the 3d printing machine and the powder materials used (SLM Solutions) [22], that confirm the obtained results (see Tab. 4), there are several scientific findings that support and validate the behavior observed for steel and nickel alloys produced by selective laser melting [16,20,21,23,24]. In particular, precipitation-hardened (17-4PH and 15-5PH stainless steels), martensite-aging steels (e.g. "maraging" 1.2709 steel) and nickel alloys Inconel 625 and 718 showed a reduction in ductility and an increase in yield and ultimate strength. In contrast, additive-manufactured aluminum and titanium alloys (AlSi10Mg aluminum alloy and Ti6Al4V titanium alloy) exhibit the same behavior as the corresponding metallic materials produced by traditional techniques [19,25–27].

Some of the specimens after the tensile test are shown in Fig. 11.

*X-ray diffraction results*

X-ray diffraction analyses have been conducted on all types of specimens to detect the presence of residual stresses (RS) and the amount of residual austenite (RA). The residual stresses were evaluated both in the parallel (90°) and in the perpendicular (0°) directions with respect to the longitudinal axis of the sample. The values of the standard deviation (SD) for specimens produced at different scanning times were also measured, as three test pieces were analyzed for each rate and only one for those with different printing orientations. The results of the XRD analysis are summarized in Tab. 11.
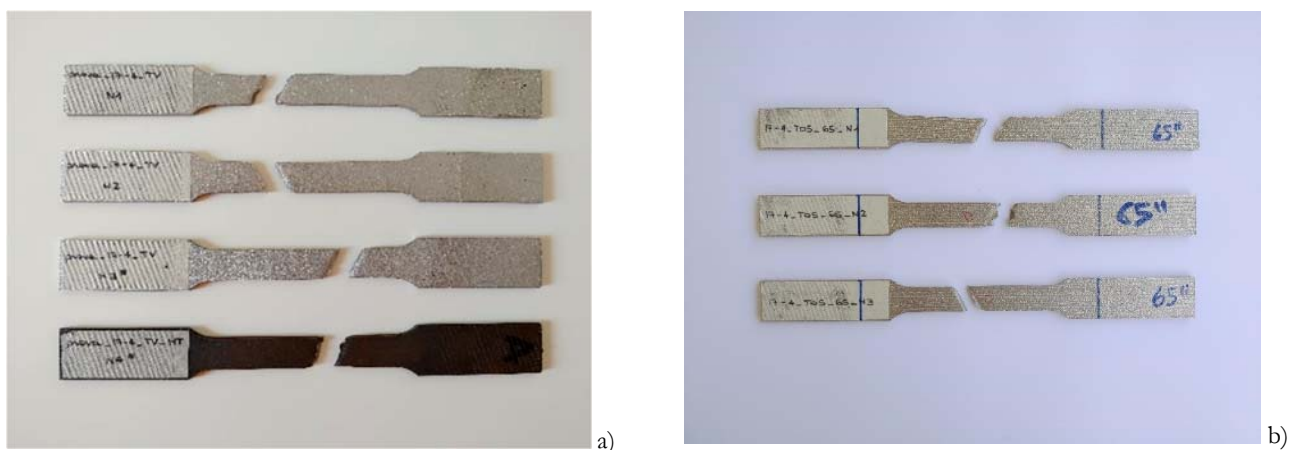


Figure 11: Location of failure of some tested 17-4PH specimens: a) Non-standardized vertically printed group; b) Standardized horizontally, 5° inclined printed group, recoating time of 65 s.

The different manufacturing strategies led to different values of residual stresses and residual austenite. The value of residual stresses for horizontally 5° inclined specimens, is 212 MPa in the parallel direction and 123 MPa in the orthogonal direction. The specimens horizontally 85° oriented are the only ones with negative residual stress values of -548 MPa in the 0° direction and -568 MPa in the other direction, which correspond to compressive residual stresses. The vertically printed specimens show residual stresses of 190 MPa in the longitudinal direction and 121 MPa in the perpendicular direction. Regarding the amount of residual austenite, the values observed are respectively 24.3%, 8.2% and 30.4% for the horizontally 5° inclined, 85° inclined and vertically produced specimens.

Conversely, the samples produced with different scanning rates do not show significant differences between the values of residual stresses and residual austenite. The results shown are average values, obtained from the three specimens tested for each category. The specimens with a scanning time of 45 s show a residual stress value of 275 MPa in the parallel direction and 116 MPa in the orthogonal direction. The samples with a scanning rate of 50 s exhibit residual stress values of 203 MPa in the 0° direction and 60 MPa in the 90° direction. The specimens produced with a scanning speed of 65 s show residual stresses of 214 MPa in the parallel direction and 44 MPa in the perpendicular one. With regard to the amount of residual austenite, the values recorded were 23.7%, 20.3% and 20.6% for specimens produced at scanning rates of 45 s, 50 s and 65 s respectively.

| Specimen ID | RS 0° MPa | SD MPa | RS 90° MPa | SD Mpa | RA % | SD % |
|---|---|---|---|---|---|---|
| G1_17-4_TO5 | 212 | / | 123 | / | 24.3 | / |
| G1_17-4_TO85 | -548 | / | -568 | / | 8.2 | / |
| G1_17-4_TV | 190 | / | 121 | / | 30.4 | / |
| G1_17-4_TO5_HT_N4 | 31 | / | 54 | / | 13.8 | / |
| G1_17-4_TO85_HT_N4 | 35 | / | 25 | / | 10.7 | / |
| G1_17-4_TV_HT_N4 | 51 | / | 21 | / | 10.2 | / |
| G2_17-4_TO5_45 | 275 | ±19 | 116 | ±14 | 23.7 | ±3.2 |
| G2_17-4_TO5_50 | 203 | ±32 | 60 | ±14 | 20.3 | ±1.6 |
| G2_17-4_TO5_65 | 214 | ±27 | 44 | ±60 | 20.6 | ±0.7 |
| G2_17-4_TO5_45_HT | 110 | ±10 | 50 | ±6 | 17.3 | ±1.4 |
| G2_17-4_TO5_50_HT | 111 | ±12 | 44 | ±7 | 11.3 | ±1.6 |
| G2_17-4_TO5_65_HT | 115 | ±28 | 46 | ±12 | 11.4 | ±0.3 |
| Powdered raw material |  |  |  |  | 35.3 |  |

Table 11: Results obtained from X-ray diffraction analysis, for both batch of specimens.

The applied heat treatment causes a homogenization and reduction of the residual stresses, independently from their manufacturing features. For horizontally 5° oriented specimens, the value of residual stresses is 31 MPa in the parallel direction and 54 MPa in the orthogonal direction (-85% and -56% compared to as-built samples). The horizontally 85° oriented specimens exhibit residual stress values of 35 MPa in the 0° direction and 25 MPa in the other direction (-106% and -104% compared to as-built samples). The vertically printed specimens show residual stresses of 51 MPa in the longitudinal direction and 21 MPa in the perpendicular direction (-73% and -83% compared to as-built samples). Regarding the amount of residual austenite, the observed values are 13.8%, 10.7% and 10.2% respectively for the horizontally 5°, 85° inclined and vertically produced specimens (-43%, +31% and -67% compared to as-built samples).
The specimens with a scanning time of 45 s show a residual stress value of 110 MPa in the parallel direction and 50 MPa in the orthogonal direction (-60% and -57% compared to as-built samples). The samples with a scanning rate of 50 s exhibit residual stress values of 111 MPa in the 0° direction and 44 MPa in the 90° direction (-45% and -26% compared to as-built samples). The specimens produced with a scanning speed of 65 s show residual stresses of 115 MPa in the parallel direction and 46 MPa in the perpendicular one (-46% and +5% compared to as-built samples). The values of residual austenite recorded were respectively 17.3%, 11.3% and 11.4% for specimens produced at scanning rates of 45 s, 50 s and 65 s (-27%, -44% and -44% compared to as-built samples). The results shown in the case of different scanning times are average values, taken from the three specimens tested for each category.

## CONCLUSIONS

In this paper, the influence of different printing orientations and inclinations, in combination with different scanning times, on the tensile properties of 17-4PH stainless steel specimens, produced via Selective Laser Melting (SLM) were investigated.
The effects of annealing treatment on the mechanical behavior of SLM-produced samples were investigated too. Moreover, in order to figure out the impact of the additive manufacturing process on the final products, the residual stresses and the amount of residual austenite were evaluated.
Based on the experimental tests, the following conclusions can be outlined:

- The applied heat treatment increased the tensile strength;
- Heat treatment reduced the failure strain and thus the ductility;
- About the first group of specimens (G1), the highest yield and fracture behavior was provided by the horizontally printed specimen inclined by 5°, both for the as-built and heat-treated samples;
- Concerning the second group of specimens (G2), the highest yield features are offered by the specimen produced with a recoating time of 45 s, both for heat-treated and as-built specimens. The highest average ultimate tensile strength values were provided by samples with a recoating time of 45 s and 50 s for as-built and annealed specimens respectively;
- The highest ductility was obtained for the specimen that was printed horizontally printed with an inclination of 5° (both for as-built and heat-treated specimens) and by samples processed with recoating times of 50 s and 65 s. The heat-treated specimens with the highest mean values of failure strain are those manufactured with a recoating time of 45 s.

## ACKNOWLEDGEMENTS

## REFERENCES

[1] Wang, J.C., Dommati, H., Hsieh, S.J. (2019). Review of additive manufacturing methods for high-performance ceramic materials, Int. J. Adv. Manuf. Technol., 103(5–8), pp. 2627–2647, DOI: 10.1007/s00170-019-03669-3.

[2] Coon, C., Pretzel, B., Lomax, T., Strlič, M. (2016). Preserving rapid prototypes: A review, Herit. Sci., 4(1), pp. 1–17, DOI: 10.1186/s40494-016-0097-y.

[3] Abdulhameed, O., Al-Ahmari, A., Ameen, W., Mian, S.H. (2019). Additive manufacturing: Challenges, trends, and applications, Adv. Mech. Eng., 11(2), pp. 1–27, DOI: 10.1177/1687814018822880.

[4] Singh, R., Gupta, A., Tripathi, O., Srivastava, S., Singh, B., Awasthi, A., Rajput, S.K., Sonia, P., Singhal, P., Saxena, K.K. (2019). Powder bed fusion process in additive manufacturing: An overview, Mater. Today Proc., 26(May), pp. 3058–3070, DOI: 10.1016/j.matpr.2020.02.635.

[5] Ligon, S.C., Liska, R., Stampfl, J., Gurr, M., Mülhaupt, R. (2017). Polymers for 3D Printing and Customized Additive Manufacturing, Chem. Rev., 117(15), pp. 10212–10290, DOI: 10.1021/acs.chemrev.7b00074.

[6] Herzog, D., Seyda, V., Wycisk, E., Emmelmann, C. (2016). Additive manufacturing of metals, Acta Mater., 117, pp. 371–392, DOI: 10.1016/j.actamat.2016.07.019.

[7] Karar, G.C., Kumar, R., Chattopadhyaya, S. (2021). An analysis on the advanced research in additive manufacturing, .

[8] Gokuldoss, P.K., Kolla, S., Eckert, J. (2017). Additive manufacturing processes: Selective laser melting, electron beam melting and binder jetting-selection guidelines, Materials (Basel)., 10(6), DOI: 10.3390/ma10060672.

[9] Carneiro, L., Jalalahmadi, B., Ashtekar, A., Jiang, Y. (2019). Cyclic deformation and fatigue behavior of additively manufactured 17–4 PH stainless steel, Int. J. Fatigue, 123(January), pp. 22–30, DOI: 10.1016/j.ijfatigue.2019.02.006.

[10] Laghi, V., Palermo, M., Gasparini, G., Girelli, V.A., Trombetti, T. (2019). Experimental results for structural design of Wire-and-Arc Additive Manufactured stainless steel members, J. Constr. Steel Res., pp. 105858, DOI: 10.1016/j.jcsr.2019.105858.

[11] Yu, Z., Zheng, Y., Chen, J., Wu, C., Xu, J., Lu, H., Yu, C. (2020). Effect of laser remelting processing on microstructure and mechanical properties of 17-4 PH stainless steel during laser direct metal deposition, J. Mater. Process. Technol., 284, pp. 116738, DOI: 10.1016/j.jmatprotec.2020.116738.

[12] Rafi, H.K., Pal, D., Patil, N., Starr, T.L., Stucker, B.E. (2014). Microstructure and Mechanical Behavior of 17-4 Precipitation Hardenable Steel Processed by Selective Laser Melting, J. Mater. Eng. Perform., 23(12), pp. 4421–4428, DOI: 10.1007/s11665-014-1226-y.

[13] Facchini, L., Vicente, N., Lonardelli, I., Magalini, E., Robotti, P., Alberto, M. (2010). Metastable austenite in 17-4 precipitation-hardening stainless steel produced by selective laser melting, Adv. Eng. Mater., 12(3), pp. 184–168, DOI: 10.1002/adem.200900259.

[14] Murr, L.E., Martinez, E., Hernandez, J., Collins, S., Amato, K.N., Gaytan, S.M., Shindo, P.W. (2012). Microstructures

and properties of 17-4 PH stainless steel fabricated by selective laser melting, J. Mater. Res. Technol., 1(3), pp. 167–177, DOI: 10.1016/S2238-7854(12)70029-7.

[15] Giganto, S., Zapico, P., Castro-Sastre, M.Á., Martínez-Pellitero, S., Leo, P., Perulli, P. (2019). Influence of the scanning strategy parameters upon the quality of the SLM parts, Procedia Manuf., 41, pp. 698–705, DOI: 10.1016/j.promfg.2019.09.060.

[16] SLM Solutions. (n.d.). Material Data Sheet Stainless Steel 17-4PH/1.4542/A564.

[17] Larimian, T., Kannan, M., Grzesiak, D., AlMangour, B., Borkar, T. (2020). Effect of energy density and scanning strategy on densification, microstructure and mechanical properties of 316L stainless steel processed via selective laser melting, Mater. Sci. Eng. A, 770(September 2019), pp. 138455, DOI: 10.1016/j.msea.2019.138455.

[18] ASTM. (2020). ASTM A370-20: Standard Test Methods and Definitions for Mechanical Testing of Steel Products, ASTM Int., , DOI: 10.1520/A0370-20.

[19] Hitzler, L., Janousch, C., Schanz, J., Merkel, M., Heine, B., Mack, F., Hall, W., Öchsner, A. (2017). Direction and location dependency of selective laser melted AlSi10Mg specimens, J. Mater. Process. Technol., 243, pp. 48–61, DOI: 10.1016/j.jmatprotec.2016.11.029.

[20] Zhang, H., Gu, D., Ma, C., Guo, M., Yang, J., Wang, R. (2019). Effect of post heat treatment on microstructure and mechanical properties of Ni-based composites by selective laser melting, Mater. Sci. Eng. A, 765(March), pp. 138294, DOI: 10.1016/j.msea.2019.138294.

[21] Sarkar, S., Kumar, C.S., Nath, A.K. (2019). Effects of heat treatment and build orientations on the fatigue life of selective laser melted 15-5 PH stainless steel, Mater. Sci. Eng. A, 755(February), pp. 235–245, DOI: 10.1016/j.msea.2019.04.003.

[22] SLM Solutions. (n.d.). Metal powder optimized for Selective Laser Melting.

[23] Yadollahi, A., Shamsaei, N., Thompson, S.M., Elwany, A., Bian, L. (2017). Effects of building orientation and heat treatment on fatigue behavior of selective laser melted 17-4 PH stainless steel, Int. J. Fatigue, 94, pp. 218–235, DOI: 10.1016/j.ijfatigue.2016.03.014.

[24] Moussaoui, K., Rubio, W., Mousseigne, M., Sultan, T., Rezai, F. (2018). Materials Science & Engineering A E ff ects of Selective Laser Melting additive manufacturing parameters of Inconel 718 on porosity, microstructure and mechanical properties, Mater. Sci. Eng. A, 735(August), pp. 182–190, DOI: 10.1016/j.msea.2018.08.037.

[25] Mower, T.M., Long, M.J. (2016). Mechanical behavior of additive manufactured, powder-bed laser-fused materials, Mater. Sci. Eng. A, 651, pp. 198–213, DOI: 10.1016/j.msea.2015.10.068.

[26] Xu, Z.W., Wang, Q., Wang, X.S., Tan, C.H., Guo, M.H., Gao, P.B. (2020). High cycle fatigue performance of AlSi10mg alloy produced by selective laser melting, Mech. Mater., 148, DOI: 10.1016/j.mechmat.2020.103499.

[27] Masuo, H., Tanaka, Y., Morokoshi, S., Yagura, H., Uchida, T. (2018). In fl uence of defects , surface roughness and HIP on the fatigue strength of Ti- 6Al-4V manufactured by additive manufacturing, Int. J. Fatigue, 117(April), pp. 163–179, DOI: 10.1016/j.ijfatigue.2018.07.020.